A step in understanding the S8 tension

Version	First author draft
Citation (published version):	M. Schmaltz, M. Joseph, D. Aloni, N. Weiner, E. Sivarajan. "A Step in Understanding the S8 Tension" Physical Review D: Particles, Fields, Gravitation and Cosmology. https://doi.org/10.48550/arXiv.2207.03500

A Step in Understanding the S_8 Tension

Melissa Joseph,[1, *] Daniel Aloni,[1, *] Martin Schmaltz,[1] Eashwar N. Sivarajan,[1] and Neal Weiner[2]

[1]*Physics Department, Boston University, Boston, MA 02215, USA*
[2]*Center for Cosmology and Particle Physics, Department of Physics,*
New York University, New York, NY 10003, USA

Models of dark sectors with a mass threshold can have important cosmological signatures. If, in the era prior to recombination, a relativistic species becomes non-relativistic and is then depopulated in equilibrium, there can be measurable impacts on the CMB as the entropy is transferred to lighter relativistic particles. In particular, if this "step" occurs near $z \sim 20,000$, the model can naturally accommodate larger values of H_0. If this stepped radiation is additionally coupled to dark matter, there can be a meaningful impact on the matter power spectrum as dark matter can be coupled via a species that becomes non-relativistic and depleted. This can naturally lead to suppressed power at scales inside the sound horizon before the step, while leaving conventional CDM signatures for power outside the sound horizon. We study these effects and show such models can naturally provide lower values of S_8 than scenarios without a step. This suggests these models may provide an interesting framework to address the S_8 tension, both in concert with the H_0 tension and without.

I. INTRODUCTION

The past two decades have seen cosmology become a precision science. A wealth of new data over wide ranges of redshifts and distance scales has appeared, allowing a precision determination of the parameters of ΛCDM. In addition, as error bars continue to shrink, we now look forward to an era where even small deviations from ΛCDM might show themselves as a statistically significant deviation in the data.

There are many reasons to expect that such deviations should appear at some point. Most models of CDM have interactions at some level, with itself and with other species, possibly within the Standard Model. Additional radiation is naturally populated by thermal contact in the early universe, although it may be proportionately small today due to the large number of degrees of the Standard Model, or some other source of entropy.

While many properties of high energy physics are hidden in the smallest scales, many different observables are sensitive to physical processes from when the photon bath had a temperature of a keV and below. Although this is much smaller than many particle physics scales, it is larger than other important scales known in nature. In particular, both the neutrino mass ($m_\nu \sim 0.1\,\mathrm{eV}$) and the cosmological constant scale ($\Lambda^4 \sim (10^{-2.5}\,\mathrm{eV})^4$) are physical scales below this. In particle physics models, there are frequently mass scales induced at scales in the several orders of magnitude around $\sim \mathrm{TeV}^2/M_{pl} \sim 10^{-4}\,\mathrm{eV}$. Thus, not only can cosmology probe the presence of additional sectors of physics, presently disconnected from ours, it probes a potentially interesting energy range, as well.

Recently, the consequences of a step in a fluid of strongly interacting radiation (SIDR) was investigated in the context of the H_0 tension [1]. The H_0 tension is the 4.8σ disagreement between the measurement of the local expansion rate based on late-universe observables, in particular Cepheid-calibrated Type IA supernovae from SH0ES [2] $H_0 = 73.04 \pm 1.04\,\mathrm{km/s/Mpc}$ when compared against inferences based early universe physics, such as from the CMB alone or in combination with BAO $H_0 = 67.27 \pm 0.60\,\mathrm{km/s/Mpc}$ [3]. A broad variety of proposals have been presented in attempts to reconcile this, see., e.g., [4–14] and additional models summarized in [15]. One common group of models include additional radiation [16–26], which may be strongly interacting. In [1], it was shown that the presence of a mass threshold in a fluid of SIDR allowed for a higher value of H_0 and a better overall fit to a broad set of data. In particular, the data preferred a mass threshold occurring near $z_t \sim 20\,000$.

The model considered there was a simple two-component model, with a massive scalar and a massless fermion. This simple model is neatly packaged in the simplest possible supersymmetric model, and was thus termed WZDR, or Wess-Zumino Dark Radiation. As the scalar becomes non-relativistic, its entropy is transferred to the fermion, heating it, and increasing the effective radiation compared to the step-less case. It is clear that extensions of this model are interesting to study. Probably the most immediately obvious to consider is the question: what if the dark matter *additionally* interacts with a portion of this dark fluid, such as, e.g., a Yukawa coupling to the scalar?

Naively, this extension would lead to a suppression of matter power for modes that were inside the horizon while the dark matter is coupled to the dark radiation fluid. In contrast, modes that come inside the horizon later would not be suppressed, leading to CDM-phenomenology on large scales, and deviations at smaller scales. The comoving horizon for modes entering at redshift z before matter radiation equality is approximately $r_s \sim 100\,\mathrm{Mpc}\,z_{eq}/z$. Thus, for the parameters which are preferred by the H_0 tension, we expect deviations from CDM on scales of $\sim 10\,h^{-1}\mathrm{Mpc}$ and below. Such a scale

---

*These authors contributed equally to this work.

is interesting in light of a separate tension, namely the S_8 tension.

Loosely speaking, the S_8 tension is the difference between more direct measurements of the level of fluctuations in the matter power spectrum on $\sim 8\,h^{-1}$Mpc scales and their prediction using ΛCDM and the CMB to normalize. More quantitatively, the directly measured values from KiDS-1000 [27] and DES Y3 [28] combined give $S_8 \equiv \sqrt{\Omega_m/0.3}\,\sigma_8 = 0.769 \pm 0.016$ which is 2.9σ lower then - for example - the value obtained from the CMB by Planck [3] $S_8 = 0.834 \pm 0.016$. Although this tension is not as statistically significant as the H_0 tension, it has appeared across many different independent measurements of S_8 [15]. Moreover, it raises a basic questions as to what sorts of models might impact the power spectrum at measurable scales, while leaving CDM-like cosmology on larger scales. The fact that a simple model extension immediately points to consequences relevant at the appropriate scale is a striking coincidence.

In this paper we will explore the consequences of dark matter interacting with a stepped fluid, where the late-time behavior after the step of dark matter is that of CDM. The layout of the paper is as follows: in Section II we lay out the specific scenarios we wish to consider, namely the WZDR model of [1] where the dark matter additionally interacts with the scalar. We study the cosmological signals of such a scenario in Section III, showing that such scenarios naturally suppress matter power on $\sim 15\,\mathrm{Mpc} \times [20\,000/z_t]$ scales and smaller. We perform a global fit in Section IV to an extended data set including a wide variety of cosmological datasets, finding a good improvement in fits compared to ΛCDM and WZDR with CDM. Finally, in Section V, we conclude. Supplementary details regarding the WZDR-DM interaction and its implementation in the Boltzmann solver, as well as a full set of posterior densities and best-fit cosmological parameters as determined by our MCMC analysis, are provided in the appendices.

II. MODEL OF A STEPPED DARK SECTOR

The Wess-Zumino Dark Radiation model (WZDR) [1] is a simple and natural example of a dark sector with a mass threshold. It contains just two particles - a fermion ψ and a scalar ϕ, which interact through a Yukawa coupling $\phi\psi\psi$. If we allow for scalar quartic interactions ϕ^4, this model is efficiently packaged into the simplest known supersymmetric model, namely, the Wess-Zumino model. Supersymmetry breaking induces a small mass $m_\phi^2\phi^2$ for the scalar, with $m_\phi \sim (M_{\mathrm{SUSY}}^2)/M_{\mathrm{pl}}$, which can naturally lie near the eV scale. Importantly, the dynamics we discuss are independent of supersymmetry, although this provides natural model-building directions.

At early times, before the CMB era, some process produces [1] the WZDR ψ and ϕ particles with an energy density equivalent to N_{UV} additional neutrino species. As ϕ and ψ always maintain chemical and kinetic equilibrium, once the temperature of this sector decreases below m_ϕ, the scalars decay and annihilate, depositing their entropy into the lighter ψ species. Due to this process which takes approximately a decade in redshift, the relative energy density of the fluid, as quantified by the effective number of additional neutrinos species $N(z)$, increases to a value $N_{\mathrm{IR}} = (15/7)^{1/3}N_{\mathrm{UV}}$. Assuming a temperature of the dark radiation today of T_{d0}, the transition approximately starts at redshift $1 + z_t = m_\phi/T_{d0}$, and the evolution of $N(z)$ as a function of redshift is calculated by solving the entropy conservation equation.

This simple model was shown to significantly alleviate the Hubble tension, with the introduction of a single low mass threshold, a "step" [1]. It is easy to imagine extensions of this model, perhaps the simplest of which is if the relativistic fluid additionally has interactions with dark matter, χ. If χ is a fermion, the simplest interaction possible is one in which an additional Yukawa coupling is added $\phi\chi\chi$. Interactions with the fluid would arise through Compton-like $\phi\chi \to \phi\chi$ processes, as well as $\chi\psi \to \chi\psi$ mediated by t-channel ϕ exchange.

Of these, the Compton-like process is typically smaller, suffering an additional T_d^2/M_χ^2 suppression. At high temperatures, $T_d \gtrsim m_\phi$, the momentum transfer rate between the DM and the WZDR sector from the t-channel process scales as [16]

$$\Gamma \propto \frac{T_d^2}{M_\chi} \qquad \text{for } T_d \gtrsim m_\phi \;, \tag{1}$$

where M_χ is the mass of the DM. Therefore during radiation domination, the momentum transfer rate scales as Hubble, and the ratio Γ/H neither increases nor decreases over time.

However, at late times, once the temperature drops below m_ϕ, the $\psi - DM$ interaction is effectively given by the four-fermi contact operator, $\psi^2\chi^2/m_\phi^2$ which gives a suppressed momentum transfer rate that scales as

$$\Gamma \propto \frac{T_d^2}{M_\chi}\left(\frac{T_d}{m_\phi}\right)^4 \qquad \text{for } T_d \lesssim m_\phi \;, \tag{2}$$

and the interaction shuts off quite rapidly after the transition time z_t.

We found that to a very good approximation the momentum transfer rate is given by the phenomenologically motivated fitting formula

$$\Gamma(x) = \Gamma_0 \frac{(1 + z_t)^2}{x^2}\left(\frac{1}{1 - 0.05\sqrt{x} + 0.131x}\right)^4 \;, \tag{3}$$

_____

[1] As discussed in Ref. [1], as we will assume here, this process can occur just after Big Bang nucleosynthesis (BBN)

where $x \equiv m_\phi/T_d$ and Γ_0 is the momentum transfer rate extrapolated to today in a theory in which there is no step (i.e. where $m_\phi = 0$). The coefficients have been chosen to best approximate the exact numerical result. A full derivation of the momentum transfer rate is given in Appendix B. From now on we will refer to a WZDR model with dark matter – dark radiation interaction that shuts off as Eq. (3) as WZDR+.

As a consequence, we have a scenario in which at early times dark matter exchanges momentum with a relativistic fluid made up of ψ and ϕ particles. This momentum transfer acts as a mild friction on the growth of matter perturbations. At late times, after z_t, we have a CDM-like χ decoupled from a still tightly self-coupled fluid of ψ. This mass threshold then naturally produces a CDM-like cosmology at late times, and a very different one beforehand.

III. EFFECTS OF A STEPPED DARK SECTOR

Stepped fluids which interact with the dark matter have interesting phenomenology, and variety of effects and imprints during the evolution of the universe. Here we discuss some of them, emphasizing that there are two distinct effects which are both sensitive to the WZDR mass scale.

The first effect which was discussed in detail in Ref. [1] is due to the increase in the effective number of degrees of freedom. Through the transition, as the energy density increases, the expansion rate of the universe increases accordingly. As a result, there is an ℓ dependent phase-shift of the CMB power spectrum compared to a model of interacting radiation without a step. To leading order there is no phase shift for small k-modes that enter the horizon after the transition, while there is a linear phase-shift for large k-modes that enter the horizon before the transition. Therefore, as the change in the behavior of the phase shift depends on the time of transition, the CMB is sensitive to m_ϕ or equivalently to z_t. Ref. [1] found that this shift is strongly preferred by the full data set including measurements of H_0 and allows for better fits with higher expansion rates.

The new ingredient of the model which we introduce here is the interaction of the stepped fluid with the dark matter. During the time of radiation domination and well before the transition the momentum transfer rate scales as Hubble, $\Gamma \propto H$, and therefore remains equally important throughout this period. Since in our model the WZDR fluid interacts with 100% of the DM, similar to the study of [16, 18], the WZDR-DM coupling is weak and the momentum transfer rate is always smaller then Hubble. As a result the DM does not oscillate but only experiences a friction as it falls into the gravitational potentials.

As explained in Ref. [18], the effect on the matter power spectrum (MPS) compared to a model with no interaction between the fluid and the DM, is a linear
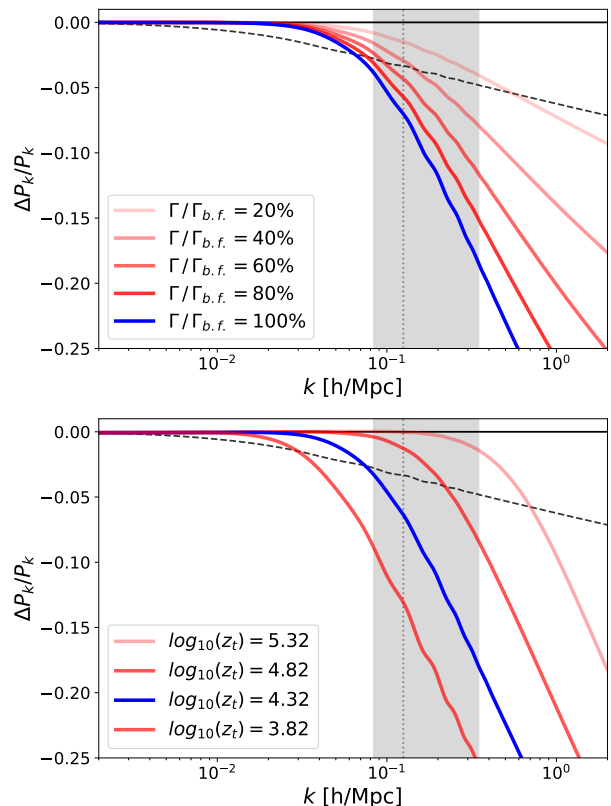

FIG. 1: Dependence of the MPS on model parameters. Both panels show ratios of the MPS in WZDR+ compared to a reference model with no DR-DM interaction. The blue line indicates the best fit point from our $\mathcal{DHS}$ fit, with $10^7\Gamma_{b.f} = 5\,\mathrm{Mpc}^{-1}$. In the top panel the different lines correspond to different interaction strengths Γ compared to the reference model with no interaction (i.e. WZDR). The bottom panel shows how the MPS varies with the redshift of the transition z_t compared to a reference model with $z_t \to \infty$. The black dashed line in both plots is the best fit of SIDR+ to the $\mathcal{DHS}$ fit compared to the same parameter space point with the DM-DR interactions shut off. The gray band shows the scales to which S_8 is most sensitive to through the σ_8 window function and the dotted gray line indicates $k = 1/8\,h\mathrm{Mpc}^{-1}$.

suppression in $\log k$ space with a slope proportional to the momentum transfer rate,

$$\frac{P_{\mathrm{interacting}}}{P_{\mathrm{not\text{-}interacting}}} \simeq \begin{cases} 1 & k \ll k_{s.o.} \\ 1 - \sqrt{2}\,\Gamma/H \times \log k/k_{s.o.} & k \gg k_{s.o.} \end{cases}.$$

Here $k_{s.o.}$ is the wave number of the mode which enters the horizon when the interaction shuts off. This effect is shown in the top panel of Figure 1, where the linear suppression is evident and the slope is proportional to the momentum transfer rate. The fact that this suppression is smooth in $\log k$ and does not introduce a sharp feature or drop-off in the MPS allows this kind of model to lower S_8 and fit the MPS extracted from Lyman-α data which prefer a steeper slope at the scale $k \sim 1\,\mathrm{Mpc}^{-1}$ [29].

In Ref. [18] the interaction becomes smaller compared

to Hubble after matter-radiation equality, as $H \propto a^{-3/2}$ while the interaction still drops as $\Gamma \propto a^{-2}$, thus the shut-off time is at the time of equality η_{eq}. In contrast, for the WZDR+ model the momentum transfer rate shuts off once the temperature drops below m_ϕ (see Eq. (3)). This is shown in the bottom panel of Figure 1. As a result the matter power spectrum, through the S_8 measurements, is sensitive to m_ϕ or equivalently to z_t.

IV. ANALYSIS

Within the WZDR+ framework, there are some immediate questions, namely: can this model give a good description of existing data? In particular, can it address the known tensions in the data? And finally, is there consistency between the different datasets in the value of z_t extracted? In this Section we consider precisely these questions. We will study how well WZDR+ can improve the overall fit to the CMB and alleviate the Hubble and S_8 tensions. Here we highlight our main results, more details from our analysis can be found in Appendices C and D.

We modified CLASS v3.1 [30] to include the stepped fluid [1] and further modified the code to include interactions with DM as described in Appendix B. We use the MontePython v3.5 [31, 32] MCMC sampler to study the constraints of various data sets on the model. Similar to Ref. [1], for the WZDR+ model, we adopt flat priors on the 6 ΛCDM cosmological parameters $\{\omega_b, \omega_{dm}, \theta_s, n_s, A_s, \tau_{reio}\}$. For the 3 new parameters of WZDR+ we include a flat prior on the amount of dark radiation after the step[2] $N_{IR} > 0.01$, a logarithmic prior on the redshift of the step location[3] $\log_{10}(z_t) \in [4.0, 4.6]$, and a linear prior on the strength of the interaction between dark radiation and dark matter $\Gamma_0 > 0$. Finally, we assume that the extra radiation in WZDR+ (and SIDR+, see below) is populated after BBN so that the predicted abundance of primordial helium Y_p is sensitive only to the Standard Model radiation at BBN ($N_{eff} = 3.044.$).

We consider combinations of three data sets:

- Our baseline data set $\mathcal{D}$ includes the Planck 2018 [3], TT,TE, and EE data for low-ℓ ('lowl_TT', 'lowl_EE') and high-ℓ ('highl_TTTEEE') with the full set of nuisance parameters. It also includes the late-universe constraints: the BAO-only likelihood ('bao_boss_dr12') from BOSS DR12 ($z = 0.38, 0.51, 0.61$)[33] and the small-z BAO likelihood ('bao_smallz_2014') including data from the 6dF

---

[2] The lower bound was included to avoid numerical issues of our code near $N_{IR} = 0$. We explicitly checked that our results are not very sensitive to small changes of this bound.
[3] These bounds are designed to avoid scanning over models in which the transition occurs too early or too late to have much effect on the CMB, see [1].

($z = 0.106$)[34] and MGS ($z = 0.15$) [35] catalogs, as well as the PANTHEON [36] supernova likelihood ('Pantheon').

- The data set $\mathcal{H}$ is chosen to test the Hubble tension, it consists of the latest measurement of the intrinsic magnitude of supernovae $M_b = -19.253 \pm 0.027$ by the SHOES collaboration [2], which we implement as a Gaussian likelihood for this parameter.

- The data set $\mathcal{S}$ is chosen to test the S_8 tension. It includes the $3 \times 2pt$ weak lensing and galaxy clustering analyses by KiDS-1000x{2dFLenS+BOSS} [27] and DES-Y3 [28] which obtain $S_8 = 0.766^{+0.020}_{-0.014}$ and $S_8 = 0.775^{+0.026}_{-0.024}$, which we implement as simple asymmetric Gaussian likelihoods for S_8. For quantifying the "Gaussian Tension" we also combine the two S_8 measurements and their positive 1σ ranges to $S_8^{direct} = 0.769 \pm 0.016$. In addition, the data set S includes the Planck lensing [3] likelihood ('Planck_lensing').

We do not include here the ACT DR4 dataset [37]. Although ACT provides the promise of great sensitivity, there are known tensions between ACT and Planck, and a thorough analysis would be needed to study the results of including potentially conflicting datasets. Given the early state of the ACT data and the promise of tremendous improvements, we defer this analysis to a separate study. We will perform fits to the combinations of data sets $\mathcal{D}$, $\mathcal{DH}$, $\mathcal{DS}$ and $\mathcal{DHS}$.

To put our fits in perspective we compare WZDR+ to two other models: ΛCDM and SIDR+, a model in which self-interacting dark radiation (SIDR) weakly interacts with the DM [16, 18]. SIDR+ is a natural model to compare to because it also has i. extra radiation which is important for the Hubble tension and ii. friction between dark radiation and dark matter which is important to address the S_8 tension; relative to WZDR+ it is just missing the mass threshold, the "step". (**DA**: A concise summary of the properties of each model is given in App. A.)

A first question to address is whether WZDR+ can provide an overall better fit to the data, and, in particular, whether it ameliorates both the H_0 and S_8 tensions simultaneously. Figure 2 shows the posterior in the $H_0 - S_8$ plane of our fit of WZDR+ to the $\mathcal{D}$ data set, i.e. without the direct measurements of H_0 or S_8. For comparison, we also show the fit of ΛCDM to the same data and the 68% and 95% confidence bands of the direct measurements in gray. One sees clearly that the posterior of WZDR+ is much wider in both H_0 and S_8 than the one for ΛCDM. In addition, the mean of the posterior for H_0 is shifted by 1.6 km/s/Mpc and the one for S_8 by 0.01. As a result the posterior now has significant overlap with the direct measurements. Note also the strongly non-Gaussian tail of the 1d posterior towards smaller values of S_8 corresponding to increasing DM-DR interaction Γ_0, and the much broader and also somewhat non-Gaussian
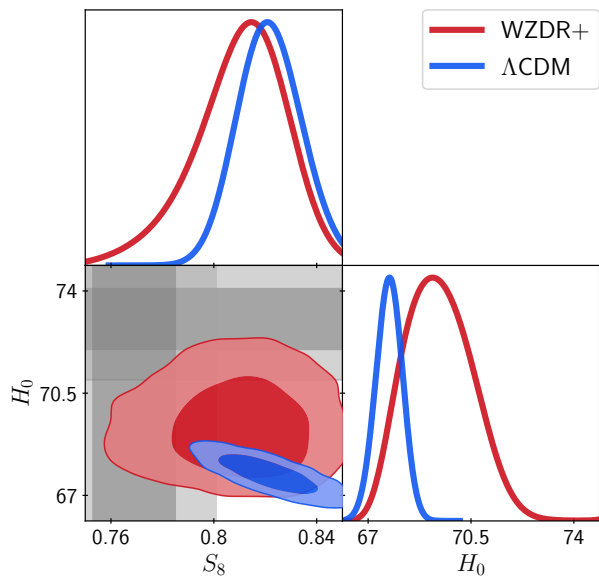
FIG. 2: Posterior distributions for ΛCDM vs. WZDR+ fitted to the data set $\mathcal{D}$. The contours of WZDR+ are much broader and in a better consistency with direct measurements of S_8 and H_0. The gray bands show the one and two sigma regions of H_0 from the SH0ES collaboration, and of our combination S_8^{direct}.
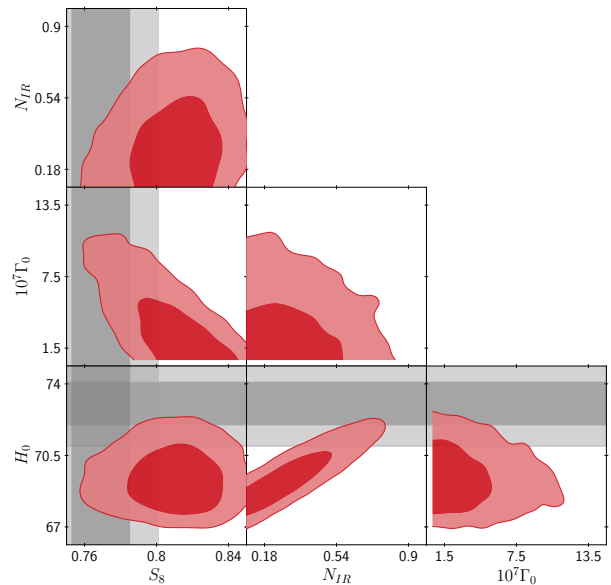

FIG. 3: Posterior distribution of WZDR+ fitted to the $\mathcal{D}$ data set. The distribution shows a clear correlation between the model parameters N_{IR} and Γ_0 and the inferred quantities H_0 and S_8. The gray bands show the one and two sigma regions of H_0 from the SH0ES collaboration, and of our combination S_8^{direct}.

1d posterior towards larger values of H_0 corresponding to increased dark radiation fluid N_{IR}. The correlations of the WZDR+ parameters N_{IR} and Γ_0 with H_0 and S_8 are clearly visible in Figure 3.

Given the broadening and shift towards larger H_0 and smaller S_8 we expect to find that the predictions for the values of these parameters in WZDR+ are in less tension with the direct measurements than in ΛCDM.

One way to quantify the tension (or lack thereof) between two data sets in a given model is to perform a combined fit to the two data sets in question and examine the goodness of fit, the χ^2. Therefore we performed fits of all three models, ΛCDM, SIDR+ and WZDR+ to the full data set $\mathcal{DHS}$. Figure 4 shows the resulting posteriors in the $\{S_8, H_0\}$ plane in blue compared with the fit to the base data set $\mathcal{D}$ (red). One sees that even with the pull from the direct measurements the ΛCDM posterior remains far from the direct measurements in H_0 and to a lesser extent in S_8. On the contrary, the much broader WZDR+ posterior from the fit to $\mathcal{D}$ overlaps both direct measurements at 1σ and almost reaches the overlap of both. Thus it is easily pulled to largely overlap with both direct measurements once fit to the full data set $\mathcal{DHS}$. The Figure shows that SIDR+ can also address both tensions, and based on the Figure alone one cannot ascertain a preference for WZDR+ versus SIDR+ or quantify the goodness of fit of either.

Thus we need to compute and compare the χ^2 values of the various best fit points to probe if they provide good overall fits to the data. Specifically, we will compute the

Q_{DMAP} value which quantifies the tension between the prediction for an observable from a fit in a model to the direct measurement by comparing the χ^2 values of the s best fit points in the fit with and without the direct measurement. For example, to determine the H_0 tension in ΛCDM, we compare the χ^2 of the s best fit point in the fit to the $\mathcal{D}$ data set, $\chi^2_{\mathcal{D}}$, to the s best fit point of the fit to the $\mathcal{DH}$ data set, $\chi^2_{\mathcal{DH}}$. The Q_{DMAP} value[4] in units of σ is then $\left(\chi^2_{\mathcal{DH}} - \chi^2_{\mathcal{D}}\right)^{1/2}$. Assuming Gaussian distributed errors the expectation for the Q_{DMAP} value in a model which perfectly describes the data is 1σ.

Table I shows the results of 3 different tests, the Q_{DMAP} for the data sets $\mathcal{DH}$, $\mathcal{DS}$, and $\mathcal{DHS}$, all compared to $\mathcal{D}$. Beginning with the first row, we see that within ΛCDM the prediction for S_8 from the fit to $\mathcal{D}$ is in moderate 2.6σ tension with the direct measurements. Much more significant at 5.6σ is the Hubble tension, the tension with the direct measurement from SH0ES.[5] The

---

[4] When the direct measurement consists of multiple measurements as in the case of S_8 one must also subtract the χ^2 due to the tension between the different direct measurements, and the Q_{DMAP} formula becomes more symmetric $\left(\chi^2_{\mathcal{DS}} - \chi^2_{\mathcal{D}} - \chi^2_{\mathcal{S}}\right)^{1/2}$. Because of the excellent agreement between the KiDS and DES measurements this correction is numerically insignificant $\chi^2_{\mathcal{S}} = 0.08$. For Gaussian posteriors the Q_{DMAP} value agree with the Gaussian Tension.

[5] This value is even larger than the 5σ tension obtained for H_0 in [2]. This is because we quantify the tension with the supernova magnitude M_b instead of H_0 which avoids the model dependence
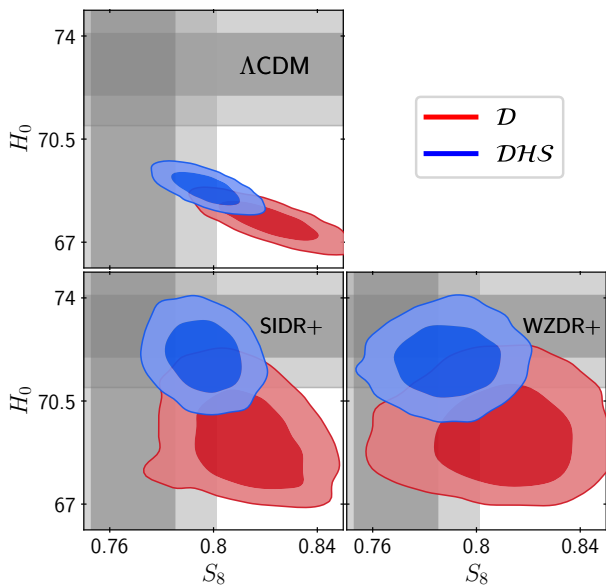
FIG. 4: Posterior distributions of ΛCDM (top left), SIDR+ (bottom left), and WZDR+ (bottom right) fitted to $\mathcal{D}$ vs. $\mathcal{DHS}$ data sets. The gray bands show the one and two sigma regions of H_0 from the SH0ES collaboration, and of our combination S_8^{direct}.

tension with both direct measurements combined is 5.8σ, and clearly ΛCDM cannot explain the combined H_0/S_8 tension.[6]

Model/Q_{DMAP}	$\mathcal{DH}$	$\mathcal{DS}$	$\mathcal{DHS}$
ΛCDM	$5.57\,\sigma$	$2.61\,\sigma$	$5.80\,\sigma$
SIDR+	$3.18\,\sigma$	$2.79\,\sigma$	$3.62\,\sigma$
WZDR+	$2.45\,\sigma$	$2.06\,\sigma$	$3.20\,\sigma$

TABLE I: Q_{DMAP} tensions

SIDR+, in contrast, makes a significant improvement in addressing the Hubble tension (which is not surprising, given the extra radiation). It does not help the S_8 tension, however, as shown by the lack of improvement in the $\mathcal{DS}$ dataset. The failure of SIDR+ to significantly reduce S_8 can be understood from Figure 1 which shows that the suppression of the MPS starts too early at $k \sim 0.01h/\mathrm{Mpc}$, which generates a tension with CMB data.[7]

_____

included in the systematic uncertainties of H_0 from [2].

[6] This is slightly smaller than the combination (in quadrature) of the Q_{DMAP} tensions for $\mathcal{DH}$ and $\mathcal{DS}$. This is due to the correlation of S_8 and H_0 visible in the ΛCDM panel of Figure 4.

[7] The SIDR+ $\mathcal{DS}$ posterior is bimodal, one mode has a minimal amount of extra radiation Nfluid ~ 0.0007 while the other has Nfluid ~ 0.07 with a local minimum of χ^2. Here we focus on the region of parameter space with $N_{\mathrm{fluid}} > 0.01$ since we are interested in the models' potential for solving both tensions.

The improvement in the $\mathcal{DHS}$ Q_{DMAP} for SIDR+ is almost entirely driven by the pull of the $\mathcal{H}$ data set and the reduction of the Hubble tension. WZDR+, on the other hand, does better in all regards, improving $\mathcal{DS}$ to a two sigma anomaly, and reducing $\mathcal{DH}$ to below three-sigma. The overall cosmological tension from both Hubble and S_8 tensions is reduced to about three-sigma. If one looks at the breakdown of χ^2 values in Appendix D, one sees that in fitting to $\mathcal{DHS}$, WZDR+ is gaining improvements from all portions of the dataset.

Another test is ΔAIC, the Akaike information criterium, which is defined as the difference of the best-fit χ^2 to all the data $\mathcal{DHS}$ between a given model and the reference ΛCDM, with a χ^2 penalty of $+2$ for each new model parameter beyond ΛCDM:

$$\Delta AIC = \chi^2 - \chi^2_{\Lambda\mathrm{CDM}} + 2 \times (\text{new parameters}) . \quad (4)$$

The results of this relatively straightforward test are shown in Table II. We see immediately that the inclusion of just a single parameter (the DM interaction strength versus WZDR, and the mass threshold versus SIDR+) improves the χ^2 by more than 5, improving the ΔAIC in each case by better than 3. This is a weak preference, to be clear, but is also reflecting the simple fact that the S_8 data are not (yet) strong enough to make this more than a tension.

	WZDR	SIDR+	WZDR+
$parameters$	2	2	3
$\Delta\chi^2$	-20.52	-19.99	-25.78
ΔAIC	-16.52	-15.99	-19.78

TABLE II: χ^2 differences and ΔAIC of WZDR, SIDR+, and WZDR+ relative to ΛCDM

Finally, there is the Gaussian Tension (GT) test. This is not an ideal test in this case because the posteriors for S_8 and the supernova magnitude M_b are not Gaussian in SIDR+ and WZDR+, but we nonetheless include the GT for completeness [8]. The posteriors for SIDR+ and WZDR+ overlap the direct measurements of S_8 and M_b at the $\sim 2-3\sigma$ level, therefore we use one half of the 2σ intervals characterizing the 1-d posteriors (these are produced in the '.h_info' files in the analysis output of MontePython). This gives a slightly better approximation to the true tension in the models than simply using the 1σ intervals.

Table III shows that the predicted value for M_b from the fit to $\mathcal{D}$ in ΛCDM has a GT of about 5.5σ to the direct measurement of M_b from SH0ES. In WZDR+ (and SIDR+) this tension is reduced to 2.6σ (2.7σ) due to the

_____

[8] The Gaussian Tension between two measurements with their 1σ errors $x_i \pm \delta x_i$ is defined as $GT = |x_1 - x_2|/\sqrt{\delta x_1^2 + \delta x_2^2}$.

interacting radiation with (and without) a step. Similarly, Table III shows a reduction of the GT in S_8 (here we compare to the combined KiDS+DES measurement) from 2.6σ in ΛCDM to 1.7σ in WZDR+ and 2.0σ in SIDR+. This reduction in S_8 is due to the DMDR interaction.[9]

Model/GT	M_b	S_8
ΛCDM	$5.5\,\sigma$	$2.6\,\sigma$
SIDR+	$2.7\,\sigma$	$2.0\,\sigma$
WZDR+	$2.6\,\sigma$	$1.7\,\sigma$

TABLE III: Gaussian Tensions.

The success we see above (in reducing the combined tensions in the data), still leaves the question whether the new ingredient - namely the transition scale - is working simultaneously to alleviate both tensions, whether they pull in different directions, or whether the improvements are really independent of each other. As was discussed in previous sections the WZDR+ model is sensitive to the mass threshold at z_t through two independent physical processes (a) via the ℓ dependence of the phase shift of the CMB due to the change in N_{eff} when T_d drops below m_ϕ, and (b) through the suppression of the matter power spectrum from the coupling between the dark matter and the dark radiation fluid due to scattering at temperatures above m_ϕ. In our previous paper we found that the CMB preferred $\log_{10}(z_t) \sim 4.3$, and it is interesting to see if this value of z_t is also preferred by the $\mathcal{DS}$ data set: the CMB power spectrum, the CMB lensing potential and the matter power spectrum at distance scales of order $k_8 \sim \text{h}/(8\text{Mpc})$ which are all sensitive to the shutoff redshift of the interaction.

To answer this question we compare the WZDR+ mean-values and best-fit points for the four data sets $\mathcal{D}, \mathcal{DH}, \mathcal{DS}$, and $\mathcal{DHS}$ and check for consistency. We

$\log_{10} z_t$	$\mathcal{D}$	$\mathcal{DH}$	$\mathcal{DS}$	$\mathcal{DHS}$
Mean	$4.35^{+0.17}_{-0.12}$	$4.29^{+0.12}_{-0.08}$	$4.38^{+0.17}_{-0.09}$	$4.32^{+0.11}_{-0.09}$
Best-fit	4.33	4.26	4.38	4.32

TABLE IV: Mean and $\pm 1\,\sigma$, and best fit values of $log10z_t$.

find the remarkable result that the value of z_t preferred by data set $\mathcal{D}$ alone (which is dominated by the CMB) is the same to within half a sigma to the preferred value for $\mathcal{DH}$, $\mathcal{DS}$ and $\mathcal{DHS}$ even though H_0 and S_8 shift by 2.8 and 1.4 sigma, respectively. We find this coincidence interesting and consider it potential evidence for the existence of a new scale $T_d \sim 10$ eV in Cosmology corresponding to redshifts of order $z_t \sim 3 \times 10^5$. This
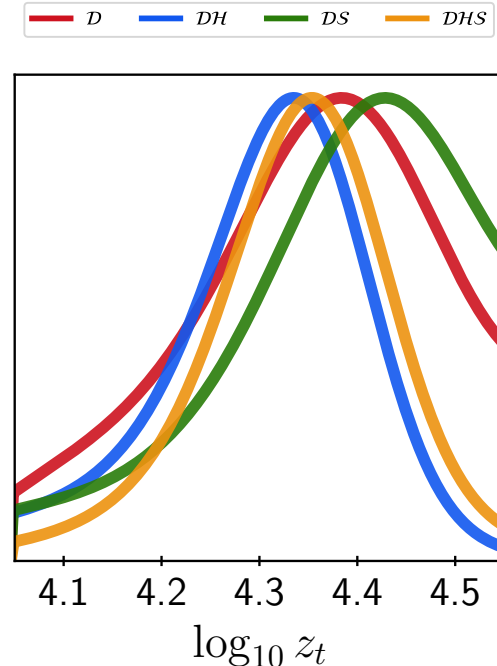
---

[9] Using the naive 1σ intervals, the GT for M_b is 5.5/3.2/3.0, and for S_8 it is 2.6/2.0/1.8 in order ΛCDM/SIDR+/WZDR+.

FIG. 5: The 1D posteriors of the transition time z_t, fitting WZDR+ to four different data sets.

coincidence can also been seen in the 1d posteriors of the variable $\log_{10}(z_t)$ for the 4 different data sets shown in Figure 5 and more concretely in the values of the best fit values of z_t seen in Table IV.

V. DISCUSSION AND OUTLOOK

In the energy range $\Lambda_{QCD} < E <$ TeV, the Standard Model has seven mass thresholds including a phase transition. Below Λ_{QCD}, the Standard Model has myriad mass thresholds from the resonances of quarks, but additionally the muon and electron masses, and at least two neutrino masses. It is somewhat striking, then, that it is commonly assumed that models of dark sectors exhibit no meaningful mass thresholds when all the physics we have ever seen is full of them.

In this vein, we have considered the effect of a single mass threshold in a dark fluid which is gently coupled to the dark matter (the WZDR+ model). The mass threshold has been previously shown to allow for enhanced H_0 with better overall fit when compared to ΛCDM or to a fluid with no mass threshold (WZDR). In particular, the Hubble tension seems to suggest a mass threshold near $z_t \sim 20,000$, when the sound horizon is approximately $10h^{-1}\text{Mpc}$.

Even without knowing this, it would be natural to consider extensions to the WZDR model where the dark radiation is coupled to the dark matter. However, noting

that the threshold occurs at a location which is precisely in the range of *another* known anomaly, namely the S_8 tension, suggests that the two anomalies - the H_0 tension and the S_8 tension, may have a common origin.

As the dark radiation passes through the mass threshold, the gentle coupling to the dark sector turns off rapidly. This can occur either because the particle with which the DM is interacting has become exponentially suppressed, or because the mediator mass is suddenly relevant, and the gentle interaction turns off. This has the natural effect of producing a CDM cosmology on large scales, and non-CDM on small scales, with the transition occurring at a scale which is singled out by the H_0 tension to be $\sim 10\,\mathrm{Mpc}$. We have seen that this scenario naturally produces a suppressed value of S_8, consistent with the directly observed value.

It is quite striking that all of the different combinations of datasets ($\mathcal{D}, \mathcal{DS}, \mathcal{DH}, \mathcal{DHS}$), all point to the same value of z_t (although the preference within $\mathcal{D}$ alone is quite small). But this is a non-trivial consistency check, without which this overall setup would be unable to reconcile these observations.

Our efforts here are the simplest extension of WZDR. One could consider multi-component dark matter where only a portion couples to the dark sector, but with enhanced interaction [18, 24]. In such a "fractional WZDR+" setup, one would expect that a similar phenomenology to the above would be found, but constraining a product of interaction strength and interacting dark matter fraction, leaving a large degeneracy. In the tightly coupled limit, the interacting dark matter fraction would acoustically oscillate, rather than feel a slight friction during infall. In this limit, one would similarly expect a good fit, but trading a precise value of Γ_0 for a precise value of the interacting fraction f_χ to fit the value of S_8. We leave the details to future work.

Beyond this, one could also imagine multiple mass thresholds, couplings to neutrinos and more. What is clear, however, is that the data, in their present form, provide sensitivity to the presence of a mass threshold in the dark sector. As data improve - both from CMB datasets of ACT, Simons Observatory and CMB-S4, as well as from LSS measurements KiDS, DES, HSC and future galaxy surveys with Rubin, Roman and UNIONS - it will become clear both whether a dark mass threshold is truly preferred by the data, and what sort of dark sector dynamics we are being pointed to.

Note added: As this work was being completed, [38] appeared, which also studies DM interacting with a WZDR fluid and includes fits to additional data. Importantly, [38] do not consider the z_t-dependent turn-off of the DM-DR interaction which we studied in this paper.

Acknowledgements

[1] D. Aloni, A. Berlin, M. Joseph, M. Schmaltz, and N. Weiner, "A Step in understanding the Hubble tension," Phys. Rev. D **105** (2022) no. 12, 123516, arXiv:2111.00014 [astro-ph.CO].

[2] A. G. Riess et al., "A Comprehensive Measurement of the Local Value of the Hubble Constant with 1 km/s/Mpc Uncertainty from the Hubble Space Telescope and the SH0ES Team," arXiv:2112.04510 [astro-ph.CO].

[3] **Planck** Collaboration, N. Aghanim et al., "Planck 2018 results. VI. Cosmological parameters," Astron. Astrophys. **641** (2020) A6, arXiv:1807.06209 [astro-ph.CO]. [Erratum: Astron.Astrophys. 652, C4 (2021)].

[4] C. Brust, Y. Cui, and K. Sigurdson, "Cosmological Constraints on Interacting Light Particles," JCAP **08** (2017) 020, arXiv:1703.10732 [astro-ph.CO].

[5] M. Escudero and S. J. Witte, "A CMB search for the neutrino mass mechanism and its relation to the Hubble tension," Eur. Phys. J. C **80** (2020) no. 4, 294, arXiv:1909.04044 [astro-ph.CO].

[6] M. Escudero Abenza and S. J. Witte, "Could the Hubble Tension be Pointing Towards the Neutrino Mass Mechanism?," in Prospects in Neutrino Physics. 4, 2020. arXiv:2004.01470 [hep-ph].

[7] M. Escudero and S. J. Witte, "The hubble tension as a hint of leptogenesis and neutrino mass generation," Eur. Phys. J. C **81** (2021) no. 6, 515, arXiv:2103.03249 [hep-ph].

[8] T. Karwal and M. Kamionkowski, "Dark energy at early times, the Hubble parameter, and the string axiverse," Phys. Rev. D **94** (2016) no. 10, 103523, arXiv:1608.01309 [astro-ph.CO].

[9] V. Poulin, T. L. Smith, T. Karwal, and M. Kamionkowski, "Early Dark Energy Can Resolve The Hubble Tension," Phys. Rev. Lett. **122** (2019) no. 22, 221301, arXiv:1811.04083 [astro-ph.CO].

[10] M.-X. Lin, G. Benevento, W. Hu, and M. Raveri, "Acoustic Dark Energy: Potential Conversion of the Hubble Tension," Phys. Rev. D **100** (2019) no. 6, 063542, arXiv:1905.12618 [astro-ph.CO].

[11] T. L. Smith, V. Poulin, and M. A. Amin, "Oscillating scalar fields and the Hubble tension: a resolution with novel signatures," Phys. Rev. D **101** (2020) no. 6,

063523, `arXiv:1908.06995 [astro-ph.CO]`.

[12] F.-Y. Cyr-Racine, F. Ge, and L. Knox, "A Symmetry of Cosmological Observables, and a High Hubble Constant as an Indicator of a Mirror World Dark Sector," `arXiv:2107.13000 [astro-ph.CO]`.

[13] K. V. Berghaus and T. Karwal, "Thermal Friction as a Solution to the Hubble and Large-Scale Structure Tensions," `arXiv:2204.09133 [astro-ph.CO]`.

[14] F. Niedermann and M. S. Sloth, "Resolving the Hubble tension with new early dark energy," Phys. Rev. D **102** (2020) no. 6, 063527, `arXiv:2006.06686 [astro-ph.CO]`.

[15] E. Abdalla et al., "Cosmology intertwined: A review of the particle physics, astrophysics, and cosmology associated with the cosmological tensions and anomalies," JHEAp **34** (2022) 49–211, `arXiv:2203.06142 [astro-ph.CO]`.

[16] M. A. Buen-Abad, G. Marques-Tavares, and M. Schmaltz, "Non-Abelian dark matter and dark radiation," Phys. Rev. D **92** (2015) no. 2, 023531, `arXiv:1505.03542 [hep-ph]`.

[17] J. Lesgourgues, G. Marques-Tavares, and M. Schmaltz, "Evidence for dark matter interactions in cosmological precision data?," JCAP **02** (2016) 037, `arXiv:1507.04351 [astro-ph.CO]`.

[18] M. A. Buen-Abad, M. Schmaltz, J. Lesgourgues, and T. Brinckmann, "Interacting Dark Sector and Precision Cosmology," JCAP **01** (2018) 008, `arXiv:1708.09406 [astro-ph.CO]`.

[19] J. L. Bernal, L. Verde, and A. G. Riess, "The trouble with H_0," JCAP **10** (2016) 019, `arXiv:1607.05617 [astro-ph.CO]`.

[20] N. Blinov and G. Marques-Tavares, "Interacting radiation after Planck and its implications for the Hubble Tension," JCAP **09** (2020) 029, `arXiv:2003.08387 [astro-ph.CO]`.

[21] S. Roy Choudhury, S. Hannestad, and T. Tram, "Updated constraints on massive neutrino self-interactions from cosmology in light of the H_0 tension," JCAP **03** (2021) 084, `arXiv:2012.07519 [astro-ph.CO]`.

[22] T. Brinckmann, J. H. Chang, and M. LoVerde, "Self-interacting neutrinos, the Hubble parameter tension, and the cosmic microwave background," Phys. Rev. D **104** (2021) no. 6, 063523, `arXiv:2012.11830 [astro-ph.CO]`.

[23] C. D. Kreisch, F.-Y. Cyr-Racine, and O. Doré, "Neutrino puzzle: Anomalies, interactions, and cosmological tensions," Phys. Rev. D **101** (2020) no. 12, 123505, `arXiv:1902.00534 [astro-ph.CO]`.

[24] Z. Chacko, Y. Cui, S. Hong, T. Okui, and Y. Tsai, "Partially Acoustic Dark Matter, Interacting Dark Radiation, and Large Scale Structure," JHEP **12** (2016) 108, `arXiv:1609.03569 [astro-ph.CO]`.

[25] G. Choi, T. T. Yanagida, and N. Yokozaki, "A model of interacting dark matter and dark radiation for H_0 and σ_8 tensions," JHEP **01** (2021) 127, `arXiv:2010.06892 [hep-ph]`.

[26] S. Bansal, J. H. Kim, C. Kolda, M. Low, and Y. Tsai, "Mirror Twin Higgs Cosmology: Constraints and a Possible Resolution to the H_0 and S_8 Tensions," `arXiv:2110.04317 [hep-ph]`.

[27] C. Heymans et al., "KiDS-1000 Cosmology: Multi-probe weak gravitational lensing and spectroscopic galaxy clustering constraints," Astron. Astrophys. **646** (2021) A140, `arXiv:2007.15632 [astro-ph.CO]`.

[28] **DES** Collaboration, T. M. C. Abbott et al., "Dark Energy Survey Year 3 results: Cosmological constraints from galaxy clustering and weak lensing," Phys. Rev. D **105** (2022) no. 2, 023520, `arXiv:2105.13549 [astro-ph.CO]`.

[29] Z. Pan, M. Kaplinghat, and L. Knox, "Searching for Signatures of Dark matter-Dark Radiation Interaction in Observations of Large-scale Structure," Phys. Rev. D **97** (2018) no. 10, 103531, `arXiv:1801.07348 [astro-ph.CO]`.

[30] D. Blas, J. Lesgourgues, and T. Tram, "The Cosmic Linear Anisotropy Solving System (CLASS) II: Approximation schemes," JCAP **07** (2011) 034, `arXiv:1104.2933 [astro-ph.CO]`.

[31] T. Brinckmann and J. Lesgourgues, "MontePython 3: boosted MCMC sampler and other features," Phys. Dark Univ. **24** (2019) 100260, `arXiv:1804.07261 [astro-ph.CO]`.

[32] B. Audren, J. Lesgourgues, K. Benabed, and S. Prunet, "Conservative Constraints on Early Cosmology: an illustration of the Monte Python cosmological parameter inference code," JCAP **02** (2013) 001, `arXiv:1210.7183 [astro-ph.CO]`.

[33] **BOSS** Collaboration, S. Alam et al., "The clustering of galaxies in the completed SDSS-III Baryon Oscillation Spectroscopic Survey: cosmological analysis of the DR12 galaxy sample," Mon. Not. Roy. Astron. Soc. **470** (2017) no. 3, 2617–2652, `arXiv:1607.03155 [astro-ph.CO]`.

[34] F. Beutler, C. Blake, M. Colless, D. H. Jones, L. Staveley-Smith, L. Campbell, Q. Parker, W. Saunders, and F. Watson, "The 6dF Galaxy Survey: Baryon Acoustic Oscillations and the Local Hubble Constant," Mon. Not. Roy. Astron. Soc. **416** (2011) 3017–3032, `arXiv:1106.3366 [astro-ph.CO]`.

[35] A. J. Ross, L. Samushia, C. Howlett, W. J. Percival, A. Burden, and M. Manera, "The clustering of the SDSS DR7 main Galaxy sample – I. A 4 per cent distance measure at $z = 0.15$," Mon. Not. Roy. Astron. Soc. **449** (2015) no. 1, 835–847, `arXiv:1409.3242 [astro-ph.CO]`.

[36] **Pan-STARRS1** Collaboration, D. M. Scolnic et al., "The Complete Light-curve Sample of Spectroscopically Confirmed SNe Ia from Pan-STARRS1 and Cosmological Constraints from the Combined Pantheon Sample," Astrophys. J. **859** (2018) no. 2, 101, `arXiv:1710.00845 [astro-ph.CO]`.

[37] **ACT** Collaboration, S. Aiola et al., "The Atacama Cosmology Telescope: DR4 Maps and Cosmological Parameters," JCAP **12** (2020) 047, `arXiv:2007.07288 [astro-ph.CO]`.

[38] N. Schöneberg and G. Franco Abellán, "A step in the right direction? Analyzing the Wess Zumino Dark Radiation solution to the Hubble tension," `arXiv:2206.11276 [astro-ph.CO]`.

[39] R. Takahashi, M. Sato, T. Nishimichi, A. Taruya, and M. Oguri, "Revising the Halofit Model for the Nonlinear Matter Power Spectrum," Astrophys. J. **761** (2012) 152, `arXiv:1208.2701 [astro-ph.CO]`.

[40] Y. Ali-Haimoud and S. Bird, "An efficient implementation of massive neutrinos in non-linear structure formation simulations," Mon. Not. Roy.

Astron. Soc. **428** (2012) 3375–3389, `arXiv:1209.0461`
`[astro-ph.CO]`.
[41] J. L. Bernal, T. L. Smith, K. K. Boddy, and
M. Kamionkowski, "Robustness of baryon acoustic
oscillation constraints for early-Universe modifications
of ΛCDM cosmology," Phys. Rev. D **102** (2020) no. 12,
123515, `arXiv:2004.07263 [astro-ph.CO]`.

Acronym	Meaning
BAO	Baryon acoustic oscillations
CDM	Cold dark matter
CMB	Cosmic microwave background
DM	Dark matter
DR	Dark radiation
MCMC	Markov chain Monte Carlo
MPS	Matter power spectrum

TABLE V: Summary of acronyms.

Appendix A: Models and Acronyms

ΛCDM - The concordance model with cosmological constant Λ and cold dark matter.

SIDR - ΛCDM + strongly self-interacting dark radiation. Dark radiation redshifts as z^4, and only the first two moments of the perturbed fluid are non-vanishing.

SIDR+ - Same as SIDR, but now the dark radiation weakly interacts with the DM. The interaction rate redshifts as Hubble during radiation domination era.

WZDR - Similar to SIDR, but the dark radiation has a mass-threshold which leads to the increase of $N_{\rm eff}$ once the temperature drops below the mass.

WZDR+ - Same as WZDR, but now the dark radiation weakly interacts with the DM. The interaction rate redshifts as Hubble during radiation domination era.

Appendix B: Momentum transfer rate

The perturbation equations for the dark matter and the WZDR fluid are sensitive to the momentum transfer rate between the two fluids. This rate is defined as $\dot{\vec{P}}_\chi = -a\Gamma \vec{P}_\chi$, the change in momentum of a DM particle P_χ due to friction it experiences while moving through the WZDR fluid of temperature T. The thermally averaged rate is given by

$$\dot{P} = \frac{a}{2E_P} \int \frac{d^3k}{(2\pi)^3\,2E_k} f(k;T) \int \frac{d^3k'}{(2\pi)^3\,2E'_k} \frac{d^3P'}{(2\pi)^3\,2E'_P} (2\pi)^4 \delta^{(4)}(P + k - P' - k') |\mathcal{M}|^2 \left(\vec{P}' - \vec{P}\right) , \qquad \text{(B1)}$$

where P, P' stands for the incoming and outgoing DM momentum, k, k' stands for a WZDR momentum, $f(k;T)$ is the thermal distribution function for the incoming scatterers from the thermal bath, and we neglect the stimulated emission/Pauli blocking term for final state particles.

As discussed in the text the $\phi - \chi$ scattering is suppressed by the massive DM propagator. Here we consider only the $\psi - \chi$ scattering mediated by t-channel ϕ exchange. The matrix element relevant for this process has the following dependence on the kinematical variables

$$|\mathcal{M}|^2 = \frac{g_{\chi\phi}^2 g_{\psi\phi}^2}{4} \frac{t(t - 4M^2)}{(t - m_\phi^2)^2} , \qquad \text{(B2)}$$

where the subscript of the coupling constants indicate the particles involved in the interaction.

Plugging this matrix element into Eq. (B1), and after some tedious algebra one finds

$$\Gamma = \tilde{\alpha}^2 \frac{T^2}{M} \int_0^\infty d\tilde{k}\,\tilde{k}^2 e^{-\tilde{k}} \int \frac{dc_\theta\,(1 - c_\theta)^2}{\left[2(1 - c_\theta) + \frac{x^2}{\tilde{k}^2}\right]^2} , \qquad \text{(B3)}$$

where $x = m_\phi/T$, and $\tilde{\alpha}$ is an effective average coupling constant normalized such that $\Gamma = \tilde{\alpha}^2 \frac{T^2}{M}$ in the case of $x = 0$. The integrals above can be evaluated analytically in terms of an awful expression with various special functions, but in all regions of interest it is approximated to a few % precision by

$$\left(\frac{1}{1 - 0.05\sqrt{x} + 0.131x}\right)^4 ,$$

where the coefficients have been tuned to approximate the exact result. Finally we parameterize the momentum transfer rate as

$$\Gamma(x) = \Gamma_0 \frac{(1 + z_t)^2}{x^2} \left(\frac{1}{1 - 0.05\sqrt{x} + 0.131x}\right)^4 , \qquad \text{(B4)}$$

where Γ_0 is the momentum transfer rate extrapolated to today in a theory in which there is no step (i.e. where $m_\phi = 0$).

With this definition the interaction rate in the UV (i.e. $T \gg m_\phi$) is $\Gamma \simeq \Gamma_0 (T_{UV}/T_0)^2 = \Gamma_0(1 + z)^2 (7/15)^{2/3}$ so

that the scattering rate in the UV is smaller than the corresponding rate in SIDR+ by $(7/15)^{2/3} \sim 0.6$.

For completeness, the momentum transfer rate enters into the dipole equations of the interacting DM and the Wess-Zumino fluid as

$$\dot{\theta}_{dm} = -\mathcal{H}\theta_{dm} + k^2\psi + a\Gamma\left(\theta_{wz} - \theta_{dm}\right) \ , \qquad \text{(B5)}$$

$$\dot{\theta}_{wz} = k^2\left(\frac{\delta_{wz}}{4} + \psi\right) - a\Gamma R\left(\theta_{wz} - \theta_{dm}\right) \ , \qquad \text{(B6)}$$

where $R \equiv 3\rho_{dm}/4\rho_{wz}$.

Appendix C: Non linear corrections

Since our fits include observables which are sensitive to the MPS at weakly non-linear scales one might wonder about the importance of non-linear effects. To probe the sensitivity of our results to non-linear physics we evaluated the χ^2 values of several of our best fit points with and without using `halofit` [39, 40]. We found slight improvements in the fits to the CMB and CMB lensing (with overall $\delta\chi^2 \sim 2 - 4$) with no significant differences in the level of improvement between models. We conclude that the impact of non-linear effects on our analysis is small and we only present results without `halofit`. We also note that S_8 is defined as an integral over the *linear* matter power spectrum which means that its sensitivity to non-linear physics is a subtlety that must be faced in the extraction of S_8 from observations, not in the theory calculation. Since `halofit` is tuned to reproduce the non-linear effects for ΛCDM it is not necessarily accurate for WZDR+ and a full analysis including non-linear effects in WZDR+ is beyond the scope of this work.

A separate concern might be that the values extracted for the BAO scale and S_8 from the data depend on non-linearities in the power spectrum. Since the experiments assumed ΛCDM in their analyses one might worry that the values for r_{BAO} and S_8 extracted would be different in our models. The BAO scale is known to be robust (for a recent analysis see [41]) against smooth changes to the MPS such as the ones predicted in our model, see Section III. Since S_8 is more sensitive to the MPS shape it would be interesting to perform a full-shape analysis in the future.

Appendix D: Triangle Plots and Parameter Values
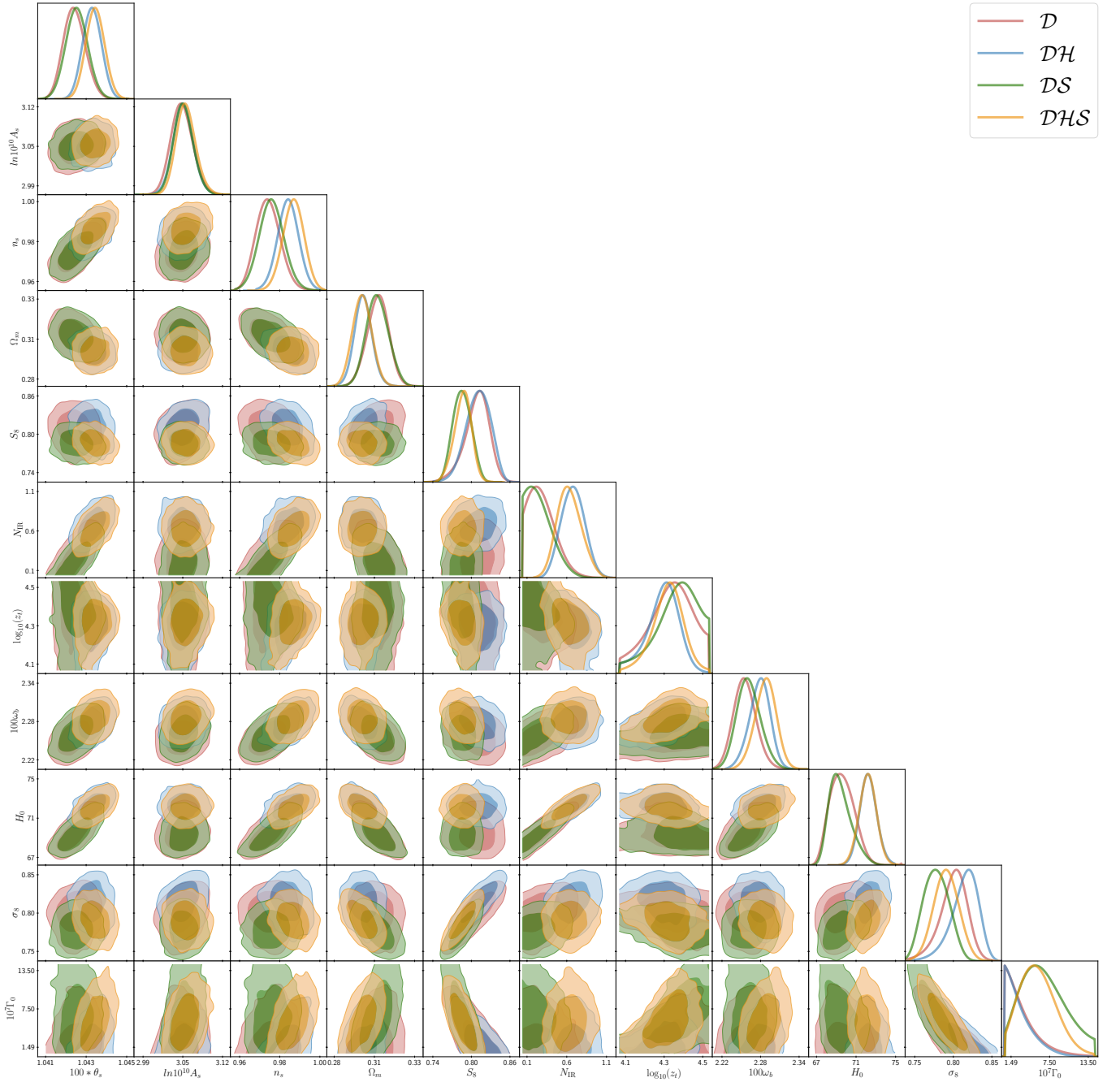
FIG. 6: A comparison of the posteriors of WZDR+ for the four different data sets. The dark and light shaded regions correspond to 68% and 95% C.L., respectively. We see that the preference for the location of the transition (z_t) is fairly consistent across the datasets possibly signaling new physics at this scale. Additionally the fit to $\mathcal{DHS}$ in comparison with the fits to $\mathcal{DH}$ and $\mathcal{DS}$ show that WZDR+ is capable of simultaneously alleviating the H_0 and S_8 tensions.
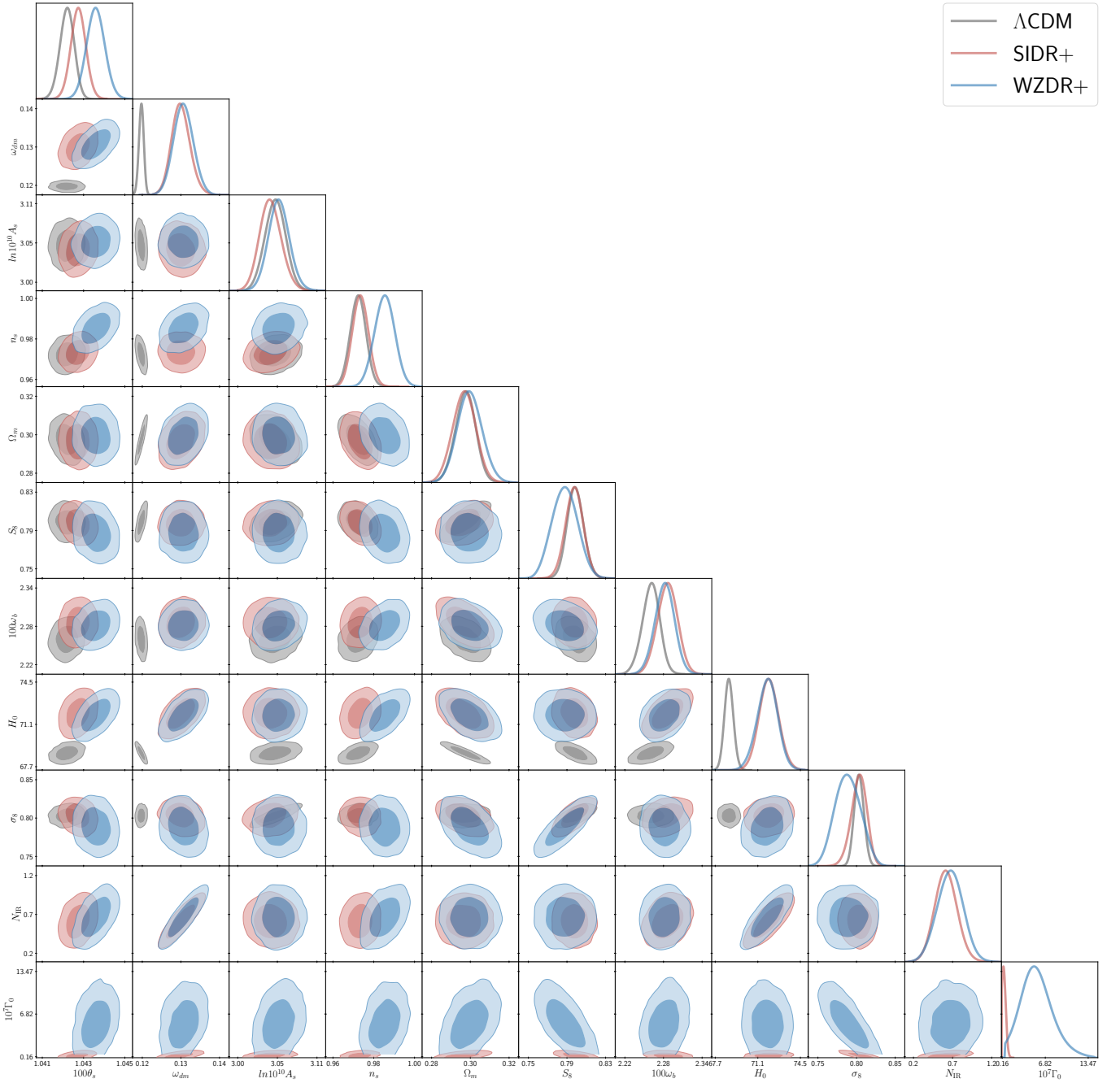
FIG. 7: A comparison of the posteriors ΛCDM, SIDR+, and WZDR+ fitting to $\mathcal{DHS}$. The dark and light shaded regions correspond to 68% and 95% C.L., respectively. From this comparison we see the importance of the step in simultaneously alleviating the H_0 and S_8 tensions. Although SIDR+ allows for larger H_0 values, it does no better than ΛCDM in resolving the S_8 tension.

	ΛCDM		SIDR+		WZDR+	
	$\mathcal{D}$	$\mathcal{D}$HS	$\mathcal{D}$	$\mathcal{D}$HS	$\mathcal{D}$	$\mathcal{D}$HS
$100\theta_s$	$1.04193^{+0.00028}_{-0.00029}$	$1.04216^{+0.00030}_{-0.00029}$	$1.04220^{+0.00031}_{-0.00034}$	$1.04261^{+0.00030}_{-0.00032}$	$1.04260^{+0.00044}_{-0.00047}$	$1.04347^{+0.00040}_{-0.00040}$
$\Omega_b h^2$	$0.02240^{+0.00014}_{-0.00014}$	$0.02263^{+0.00013}_{-0.00014}$	$0.02254^{+0.00016}_{-0.00020}$	$0.02288^{+0.00015}_{-0.00015}$	$0.02256^{+0.00016}_{-0.00017}$	$0.02287^{+0.00016}_{-0.00016}$
$\Omega_{\rm dm} h^2$	$0.11911^{+0.00097}_{-0.00098}$	$0.11678^{+0.0079}_{-0.0082}$	$0.1237^{+0.0024}_{-0.0038}$	$0.1295^{+0.0028}_{-0.0032}$	$0.1244^{+0.0025}_{-0.0038}$	$0.1305^{+0.0031}_{-0.0034}$
$\ln 10^{10} A_s$	$3.045^{+0.015}_{-0.017}$	$3.050^{+0.015}_{-0.015}$	$3.043^{+0.017}_{-0.018}$	$3.043^{+0.015}_{-0.017}$	$3.050^{+0.015}_{-0.018}$	$3.057^{+0.014}_{-0.017}$
n_s	$0.9662^{+0.0039}_{-0.0038}$	$0.9717^{+0.0038}_{-0.0035}$	$0.9681^{+0.0040}_{-0.0038}$	$0.9727^{+0.0037}_{-0.0037}$	$0.9742^{+0.0052}_{-0.0057}$	$0.9861^{+0.0051}_{-0.0048}$
$\tau_{\rm reio}$	$0.0558^{+0.0075}_{-0.0080}$	$0.0602^{+0.0077}_{-0.0077}$	$0.0563^{+0.0077}_{-0.0084}$	$0.0601^{+0.0072}_{-0.0083}$	$0.0568^{+0.0073}_{-0.0082}$	$0.0587^{+0.0069}_{-0.0082}$
$N_{\rm IR}$	-	-	$0.252^{+0.068}_{-0.239}$	$0.63^{+0.14}_{-0.14}$	$0.29^{+0.10}_{-0.24}$	$0.67^{+0.15}_{-0.16}$
$10^7 \Gamma_0$ [1/Mpc]	-	-	$0.254^{+0.060}_{-0.254}$	$0.43^{+0.16}_{-0.38}$	$2.95^{+0.63}_{-2.95}$	$5.7^{+2.4}_{-3.4}$
$\log_{10}(z_t)$	-	-	-	-	$4.35^{+0.17}_{-0.11}$	$4.322^{+0.106}_{-0.088}$
$\sigma8$	$0.8085^{+0.0070}_{-0.0073}$	$0.8031^{+0.0058}_{-0.0060}$	$0.8032^{+0.0132}_{-0.0096}$	$0.8029^{+0.0110}_{-0.0090}$	$0.800^{+0.020}_{-0.013}$	$0.791^{+0.016}_{-0.016}$
Ω_m	$0.3101^{+0.0058}_{-0.0060}$	$0.2956^{+0.0046}_{-0.0048}$	$0.3068^{+0.0067}_{-0.0068}$	$0.2950^{+0.0051}_{-0.0054}$	$0.3078^{+0.0066}_{-0.0065}$	$0.2983^{+0.0057}_{-0.0059}$
M_b	$-19.417^{+0.013}_{-0.012}$	$-19.388^{+0.010}_{-0.011}$	$-19.371^{+0.026}_{-0.041}$	$-19.290^{+0.023}_{-0.024}$	$-19.368^{+0.026}_{-0.038}$	$-19.294^{+0.023}_{-0.024}$
H_0 [km/s/Mpc]	$67.71^{+0.45}_{-0.44}$	$68.83^{+0.38}_{-0.37}$	$69.22^{+0.88}_{-1.37}$	$72.03^{+0.80}_{-0.81}$	$69.29^{+0.93}_{-1.21}$	$71.86^{+0.79}_{-0.83}$
S_8	$0.822^{+0.012}_{-0.013}$	$0.7972^{+0.0087}_{-0.0088}$	$0.812^{+0.015}_{-0.014}$	$0.7962^{+0.0097}_{-0.0094}$	$0.810^{+0.020}_{-0.016}$	$0.7889^{+0.0014}_{-0.0013}$

TABLE VI: Mean and $\pm 1\sigma$ values for a fit to dataset $\mathcal{D}$ and $\mathcal{D}\mathcal{H}\mathcal{S}$.

	ΛCDM		SIDR+		WZDR+	
	$\mathcal{D}$	$\mathcal{D}$HS	$\mathcal{D}$	$\mathcal{D}$HS	$\mathcal{D}$	$\mathcal{D}$HS
$100\theta_s$	1.04193	1.04217	1.04196	1.04256	1.04251	1.04347
$\Omega_b h^2$	0.02239	0.02265	0.02247	0.02287	0.02255	0.02286
$\Omega_{\rm cdm} h^2$	0.11925	0.11685	0.11997	0.12868	0.1243	0.1307
$\ln 10^{10} A_s$	3.044	3.052	3.044	3.039	3.047	3.053
n_s	0.9666	0.9735	0.9677	0.9721	0.9735	0.9867
$\tau_{\rm reio}$	0.0547	0.0608	0.0560	0.05870	0.0561	0.0574
$N_{\rm IR}$	-	-	0.057	0.60	0.30	0.67
$10^7 \Gamma_0$ [1/Mpc]	-	-	0.001	0.296	0.050	4.99
$\log_{10}(z_t)$	-	-	-	-	4.33	4.32
$\sigma8$	0.8085	0.8049	0.8094	0.8060	0.8203	0.7937
Ω_m	0.3109	0.2959	0.3081	0.2941	0.3057	0.2987
M_b	-19.419	-19.387	-19.404	-19.292	-19.364	-19.294
H_0 [km/s/Mpc]	67.64	68.82	68.15	71.93	69.46	71.84
S_8	0.823	0.799	0.820	0.7981	0.828	0.7920
$\chi^2_{\rm CMB}$	2767.08	2773.04	2767.20	2774.48	2766.15	2771.55
$\chi^2_{\rm Pantheon}$	1025.93	1025.73	1025.80	1025.74	1025.72	1025.64
$\chi^2_{\rm BAO}$	5.65	6.14	5.32	6.58	5.14	5.67
$\chi^2_{\rm Pl.\ lensing}$	(9.07)	10.37	(9.13)	11.31	(9.30)	10.43
$\chi^2_{\rm S8}$	(11.59)	3.65	(10.41)	3.36	(13.77)	2.12
$\chi^2_{\rm SH0ES}$	(37.64)	24.61	(31.21)	2.08	(16.81)	2.34
$\chi^2_{\rm tot}$	3798.66	3843.54	3798.33	3823.55	3797.01	3817.76

TABLE VII: Best-fit values for a fit to dataset $\mathcal{D}$ and $\mathcal{D}\mathcal{H}\mathcal{S}$.

	$\mathcal{D}$	$\mathcal{D}$H	$\mathcal{D}$S	$\mathcal{D}$HS
$100\theta_s$	$1.04260^{+0.00044}_{-0.00047}$	$1.04334^{+0.00038}_{-0.00039}$	$1.04268^{+0.00043}_{-0.00052}$	$1.04347^{+0.00040}_{-0.00040}$
$\Omega_b h^2$	$0.02256^{+0.00016}_{-0.00017}$	$0.02278^{+0.00017}_{-0.00015}$	$0.02263^{+0.00016}_{-0.00019}$	$0.02287^{+0.00016}_{-0.00016}$
$\Omega_{\rm dm} h^2$	$0.1244^{+0.0025}_{-0.0038}$	$0.1311^{+0.0030}_{-0.0030}$	$0.1241^{+0.0025}_{-0.0040}$	$0.1304^{+0.0031}_{-0.0034}$
$\ln 10^{10} A_s$	$3.050^{+0.015}_{-0.018}$	$3.052^{+0.016}_{-0.017}$	$3.052^{+0.014}_{-0.017}$	$3.057^{+0.014}_{-0.017}$
n_s	$0.9742^{+0.0052}_{-0.0057}$	$0.9836^{+0.0047}_{-0.0050}$	$0.9758^{+0.0056}_{-0.0063}$	$0.9861^{+0.0051}_{-0.0048}$
$\tau_{\rm reio}$	$0.0568^{+0.0073}_{-0.0082}$	$0.0578^{+0.0073}_{-0.0085}$	$0.0570^{+0.0072}_{-0.0080}$	$0.0587^{+0.0069}_{-0.0082}$
$N_{\rm IR}$	$0.29^{+0.10}_{-0.24}$	$0.71^{+0.14}_{-0.16}$	$0.266^{+0.069}_{-0.253}$	$0.67^{+0.15}_{-0.16}$
$10^7 \Gamma_0$ [1/Mpc]	$2.95^{+0.63}_{-2.95}$	$2.68^{+0.60}_{-2.68}$	$6.6^{+2.8}_{-4.3}$	$5.7^{+2.4}_{-3.4}$
$\log_{10}(z_t)$	$4.35^{+0.17}_{-0.11}$	$4.290^{+0.118}_{-0.081}$	$4.381^{+0.167}_{-0.095}$	$4.322^{+0.106}_{-0.088}$
$\sigma 8$	$0.800^{+0.020}_{-0.013}$	$0.813^{+0.020}_{-0.013}$	$0.779^{+0.015}_{-0.017}$	$0.791^{+0.016}_{-0.016}$
Ω_m	$0.3078^{+0.0066}_{-0.0065}$	$0.2989^{+0.0060}_{-0.0055}$	$0.3074^{+0.0066}_{-0.0064}$	$0.2983^{+0.0057}_{-0.0059}$
M_b	$-19.368^{+0.026}_{-0.038}$	$-19.291^{+0.023}_{-0.025}$	$-19.369^{+0.025}_{-0.040}$	$-19.294^{+0.023}_{-0.024}$
H_0 [km/s/Mpc]	$69.29^{+0.93}_{-1.21}$	$71.92^{+0.78}_{-0.87}$	$69.27^{+0.84}_{-1.31}$	$71.86^{+0.79}_{-0.83}$
S_8	$0.810^{+0.020}_{-0.016}$	$0.812^{+0.020}_{-0.017}$	$0.788^{+0.013}_{-0.013}$	$0.7889^{+0.0014}_{-0.0013}$

TABLE VIII: Mean and $\pm 1\sigma$ values for a fits of WZDR+.

	$\mathcal{D}$	$\mathcal{D}$H	$\mathcal{D}$S	$\mathcal{D}$HS
$100\theta_s$	1.04251	1.04321	1.04258	1.04347
$\Omega_b h^2$	0.02255	0.00227	0.02260	0.02286
$\Omega_{\rm dm} h^2$	0.1243	0.1303	0.1228	0.1307
$\ln 10^{10} A_s$	3.047	3.053	3.052	3.053
n_s	0.9735	0.9813	0.9754	0.9867
$\tau_{\rm reio}$	0.0561	0.0584	0.0570	0.0574
$N_{\rm IR}$	0.30	0.70	0.21	0.67
$10^7 \Gamma_0$ [1/Mpc]	0.05	0.43	4.84	4.99
$\log_{10}(z_t)$	4.33	4.26	4.38	4.32
$\sigma 8$	0.8203	0.8308	0.7836	0.7937
Ω_m	0.3057	0.2980	0.3068	0.2987
M_b	-19.364	-19.293	-19.377	-19.294
H_0 [km/s/Mpc]	69.46	71.83	69.01	71.84
S_8	0.828	0.828	0.792	0.792
$\chi^2_{\rm CMB}$	2766.15	2769.30	2768.20	2771.55
$\chi^2_{\rm Pantheon}$	1025.72	1025.71	1025.75	1025.64
$\chi^2_{\rm BAO}$	5.14	5.81	5.18	5.67
$\chi^2_{\rm Pl.\ lensing}$	(9.30)	(9.75)	9.81	10.43
$\chi^2_{\rm S8}$	(13.77)	(13.82)	2.19	2.12
$\chi^2_{\rm SH0ES}$	(16.81)	2.20	(21.22)	2.34
$\chi^2_{\rm tot}$	3797.01	3803.02	3811.13	3817.76

TABLE IX: Best-fit values for a fits of WZDR+.

	ΛCDM				SIDR+				WZDR+			
	H0	S_8	$\chi^2_{\min}$	Q_{DMAP}	H0	S_8	$\chi^2_{\min}$	Q_{DMAP}	H0	S_8	$\chi^2_{\min}$	Q_{DMAP}
$\mathcal{D}$	67.64	0.823	3798.66		68.15	0.820	3798.33		69.46	0.828	3797.01	
$\mathcal{DH}$	68.63	0.802	3829.68	$5.57\,\sigma$	71.74	0.808	3808.46	$3.18\,\sigma$	71.83	0.828	3803.03	$2.45\,\sigma$
$\mathcal{DS}$	68.32	0.802	3805.45	$2.61\,\sigma$	69.25	0.794	3806.10	$2.79\,\sigma$	69.49	0.787	3801.26	$2.06\,\sigma$
$\mathcal{DHS}$	68.96	0.790	3832.32	$5.80\,\sigma$	72.03	0.791	3811.47	$3.62\,\sigma$	71.86	0.790	3807.23	$3.20\,\sigma$

TABLE X: Best-fit points used for calculating the Q_{DMAP} values. Note that for the data sets $\mathcal{DS}$ and $\mathcal{DHS}$ in this table and in the resulting Q_{DMAP} values only we excluded the Planck Lensing likelihood from the $\mathcal{S}$ data set. This was done because it is not straightforward to define Q_{DMAP} with it included in $\mathcal{S}$. Here $Q_{DMAP}(\mathcal{DX}) = \left(\chi^2_{\mathcal{DX}} - \chi^2_{\mathcal{D}}\right)^{1/2}$ for $\mathcal{X} = \mathcal{H}, \mathcal{S}, \mathcal{HS}$.